Proposal to assess printability of bioinks for extrusion-based bioprinting and evaluation of rheological properties governing bioprintability

Proposal to assess printability of bioinks for extrusion-based bioprinting and evaluation of rheological properties governing bioprintability

Biofabrication

PAPER

Proposal to assess printability of bioinks for extrusion-based bioprinting and evaluation of rheological properties governing bioprintability

Naomi Paxton[1,2], Willi Smolan[1], Thomas Böck[1], Ferry Melchels[3], Jürgen Groll[1,4] and Tomasz Jungst[1,4]

[1] Department for Functional Materials in Medicine and Dentistry and Bavarian Polymer Institute, Julius-Maximilians-Universität Würzburg, Germany
[2] Institute of Health and Biomedical Innovation, Queensland University of Technology (QUT), Brisbane, Australia
[3] Institute of Biological Chemistry, Biophysics and Bioengineering, Heriot-Watt University, Edinburgh, United Kingdom
[4] Author to whom any correspondence should be addressed.

E-mail: juergen.groll@fmz.uni-wuerzburg.de **and** tomasz.juengst@fmz.uni-wuerzburg.de

Keywords: bioprinting, rheology, modelling, bioink

Supplementary material for this article is available online

OPEN ACCESS

RECEIVED
23 May 2017

REVISED
17 August 2017

ACCEPTED FOR PUBLICATION
20 September 2017

PUBLISHED
14 November 2017

Abstract

The development and formulation of printable inks for extrusion-based 3D bioprinting has been a major challenge in the field of biofabrication. Inks, often polymer solutions with the addition of crosslinking to form hydrogels, must not only display adequate mechanical properties for the chosen application but also show high biocompatibility as well as printability. Here we describe a reproducible two-step method for the assessment of the printability of inks for bioprinting, focussing firstly on screening ink formulations to assess fibre formation and the ability to form 3D constructs before presenting a method for the rheological evaluation of inks to characterise the yield point, shear thinning and recovery behaviour. In conjunction, a mathematical model was formulated to provide a theoretical understanding of the pressure-driven, shear thinning extrusion of inks through needles in a bioprinter. The assessment methods were trialled with a commercially available crème, poloxamer 407, alginate-based inks and an alginate-gelatine composite material. Yield stress was investigated by applying a stress ramp to a number of inks, which demonstrated the necessity of high yield for printable materials. The shear thinning behaviour of the inks was then characterised by quantifying the degree of shear thinning and using the mathematical model to predict the window of printer operating parameters in which the materials could be printed. Furthermore, the model predicted high shear conditions and high residence times for cells at the walls of the needle and effects on cytocompatibility at different printing conditions. Finally, the ability of the materials to recover to their original viscosity after extrusion was examined using rotational recovery rheological measurements. Taken together, these assessment techniques revealed significant insights into the requirements for printable inks and shear conditions present during the extrusion process and allow the rapid and reproducible characterisation of a wide variety of inks for bioprinting.

1. Introduction

Over the last few years, biofabrication has gained significant attention. In this relatively young field of research, automated assembly or additive manufacturing technologies are exploited to generate hybrid cell-material 3D constructs with predetermined positioning of both materials and cells [1]. This approach holds great promises to offer solutions for some of the enduring and yet unsolved challenges in tissue engineering and regenerative medicine, such as vascularisation or innervation. Researchers from different scientific backgrounds try to solve some of the main bottlenecks of this highly interdisciplinary research field. Amongst other challenges, the availability of suitable materials used for the fabrication of hierarchical, complex constructs is one of the main bottlenecks limiting the development of biofabrication. Here,

bioinks consisting of both biomaterials and cells are especially interesting and are believed to help introducing the hierarchy needed to generate constructs mimicking the complexity of natural tissues. The most prominent class of materials for bioinks are hydrogels because they can provide a viable microenvironment for the attachment, growth and proliferation of cells [2]. In addition to tuning the biological and mechanical properties of these gels to enhance cell viability and mechanical performance, they also must be printable. Printability is defined by the rheological properties of the materials and must be adjusted to the fabrication process used to generate constructs with high shape fidelity.

The main biofabrication techniques for processing of bioinks are inkjet printing, laser-induced forward transfer and extrusion-based bioprinting [3–5]. Extrusion-based bioprinting in particular is popular amongst bioink developers because it is the most versatile process, enables the broadest range of bioink viscosities to be processed and most suitably allows for printing at clinically relevant throughput [3]. In addition, devices are commercially available and, by changing extrusion nozzle diameters, they are also easily adaptable to the properties of newly developed materials. Most systems use pressurised air for dispensing and are equipped with single-use tubular or conical nozzles with varying inner diameters.

Although extrusion-based bioprinting offers a flexible fabrication platform, the rheological demands placed on the bioinks are stringent. Rheological analysis can help to accelerate the development of printable materials and many groups demonstrate useful characterisation techniques and also introduce mathematical models which help to gain a deeper understanding for the printability of materials based on rheological analysis [6]. Droplet-based printing techniques have been amongst the first techniques used in bioprinting [7] and the demands on rheological properties of bioinks used for drop-on-demand techniques have been nicely described in the literature both for inkjet [8] and valve-based [9] approaches. For example, recent publications from Sarker *et al* [10] and Kraut *et al* [11] show excellent rheological analysis of established and new inks formulations introducing robust and simple non-Newtonian fluid models derived from other research areas including the food industry [12] and electronics packaging [13, 14]. However, characterisation experiments often lack comparability and transferability to materials with unknown printing properties. Especially for scientists transitioning into the field of biofabrication, comparable, reproducible and efficient characterisation techniques for the printability of bioinks would be a decisive advantage.

Furthermore, the interdisciplinary nature of biofabrication has hindered the understanding of interactions between material properties, printability and cytocompatibility. Active discussions in the field of biofabrication focus on cell survival using extrusion-based printing processes and could benefit from a better understanding of these interactions. It is believed that the main cause for cell damage and loss of overall viability is the shear forces present in the needle during printing. Insightful work on this topic was reported by the group of Wei Sun [15–17] among other publications which also addressed this topic [9]. A very interesting publication even modelled the mechanical cell damage during bioprinting [18]. Besides optimising the printing process itself, for example by using crosslinking approaches that enable processing low viscosity materials [19, 20], the material properties can influence shear rates generated in the dispensing nozzles [20, 21]. Due to the complexity of rheological analysis and the established models, a rapid approach improving the general understanding of cell damage during dispensing will be beneficial for material scientists and biologist to improve cell survival by adapted material design.

The main focus of this publication is to support scientists starting to develop bioinks and accelerate the transition from material concept to printable ink. This study aims to propose and validate an experimental method for the initial screening and rheological evaluation of bioinks with a broad spectrum of materials properties to determine printability. We demonstrate that using a simple hand-extrusion screening process, inks can rapidly be screened to determine useful concentration, composition and crosslinking application for fibre formation and layer stacking ability. Beyond this easy to perform printability assessment, we show how shear-viscosity rheometry combined with theoretical modelling can be used to determine applicable bioprinting conditions and provide useful insight into cell survival and the final stability of the bioprinted constructs. We hypothesise that this combination of material characterisation and modelling can be extended to other bioinks and that this more integral approach may evolve into a true assessment of bioprintability including cell survival.

2. Materials and methods

2.1. Ink formation

Nivea Crème (Beiersdorf Global AG, Germany) was used as purchased. Poloxamer 407 inks were purchased from Sigma Aldrich and processed by mixing Poloxamer 407 powder (Pluronic F127, P2443-250G, Sigma Aldrich) in 10–30 wt% solutions with H_2O (MilliQ). Samples were refrigerated for 24 h at 5 °C and transferred into 1 ml syringes (NORM-JECT Tuberkulin, Henke Sass Wolf, Germany) prior to testing. Additionally, a range of concentrations of alginate polymer solutions were formulated by mixing sodium alginate powder (Protanal LF 10/60 FT, FMC BioPolymer, USA) in 10% w/v solution with 10% w/v concentration phosphate buffered saline (PBS).

Samples were pre-crosslinked with 0%–2% w/v $CaCl_2$ solution (102392 calcium chloride, Merck Millipore, USA) in a 7:3 volume mixing ratio. Samples were stored at 37 °C for 24 h and transferred into 1 ml syringes prior to testing. An alginate-gelatine blend hydrogel was prepared by mixing a 4% w/v alginate hydrogel, method as above, and a 20% w/v gelatine (G1890-100G Gelatine from porcine skin, Sigma Aldrich, USA) hydrogel, both in PBS solution. After 2 h of storage at 37 °C, the two gels are mixed together and stored again for 2 h to mix thoroughly before being transferred into a 1 ml syringe [22]. All samples were then centrifuged to remove air bubbles for 5 min at 25 °C and 4500 rpm (3893 g).

2.2. Initial screening: fibre formation and layer stacking analysis

For each sample, a 125 μm radius needle was attached to the end of the 1 ml syringe. Pressure was manually placed on the plunger until material was extruded. Images were taken using a contact angle measurement device (OCA 20, DataPhysics Instruments GmbH, Germany). The patterns used to investigate layer stacking were drawn manually and imaged with a stereomicroscope (Carl Zeiss SteREO Discovery.V20).

2.3. Rheological evaluations

A Physica MCR301 rheometer (Anton Paar, Ostfildern, Germany) was used with plate–plate geometry (25, 0.5 mm distance) and a solvent trap to prevent drying. For all materials, a shear stress ramp, ranging from 0.01 to 100 Pa was applied to each material and the yield point was defined as the intersection point between two linear regressions at the plateau-region and viscosity-drop regions of the viscosity-shear stress diagrams, indicating the point at which the material first started to flow. Rotational shear-viscosity measurements were performed in flow mode with shear rate ranging from 0.01 to 2000 s^{-1} or to the highest shear rate achievable before material was lost out of the plate–plate system. Rotational recovery measurements were performed to characterise the materials recovery behaviour by applying a low shear rate of 0.01 s^{-1} for 200 s, following by a high shear rate at 895 s^{-1} for 100 s and finally a low shear rate of 0.01 s^{-1} for 200 s. For all materials except the alginate-gelatine sample, measurements were performed at 24 °C, while for the alginate-gelatine, measurements were performed at 37 °C. Additional characterisation of the alginate-gelatine sample involved performing a temperature ramp between 20 °C and 40 °C at a shear rate of 50 s^{-1} to characterise the thermoresponsive properties of the alginate-gelatine ink.

2.4. Bioprinting

The bioprinter used in this investigation is a multi-headed 3D Discovery bioprinter (RegenHU, Switzerland). For ink extrusion, the DD135N air pressure extruder (PH2) was used with a variety of needle sizes, pressures and collector plate speeds, optimised for each material. The print-head was kept at room temperature for all samples except the alginate-gelatine hydrogel where a heater and cooling plate were used to assist deposition and solidification. Materials were loaded into a 3CC printing syringe (Nordson EFD, USA) and mounted into the printer with the pressure hose attached above and needle below. All needles used in the project were purchased from Nordson EFD 'general purpose' 0.25' dispensing tips, 12.22 mm in length metal needles with inner diameters ranging from 0.2 to 0.33 mm. Completed alginate-based scaffolds were submerged in 2% w/v calcium chloride ($CaCl_2$) solution for 30 s before being washed in H_2O. All samples except the alginate-gelatine composite were printed at room temperature, 24 °C, onto a room temperature glass microscope slide. A pressure-assisted microvalve print-head (PH1, CF-300N/H) was used to print the alginate-gelatine sample, along with a cartridge heater (CF300, RegenHU, Switzerland) and custom cooling plate set up to maintain the bioink in the syringe at 30 °C and cool the collector plate to 10 °C.

Gcode for square scaffolds, 12 × 12 mm in dimension, was produced with crosshatch infill with 1.5 mm spacing between fibres. Initially, the printing height of the needle above the collector plate was found by measuring the 'zero' position where the needle is in contact with the collector plate and then raising it by 2/3 of the needle diameter. During printing, this was then further optimised to create well-attached, round, consistent fibres. Where poor attachment or inconsistency was observed, the initial height was lowered, while flattened, squashed fibres indicated the printing height needed to be raised. To optimise the extrusion parameters, the pressure was initially set by observing the flow of material out of the needle in a stationary position. The starting pressure was determined to be when a steady fibre flow was produced. Initially, the collector plate velocity was set to 10 mm s^{-1} and then optimised based on the quality and accuracy of fibre deposition. If the corners of the crosshatch pattern were not maintained, the speed was too high and had to be lowered. Conversely, if too much material was being deposited, leading to thick, non-circular fibres, the pressure and/or collector plate velocity was lowered. Completed scaffolds were imaged using a stereomicroscope (Carl Zeiss SteREO Discovery.V20).

2.5. Cell culture and bioink formation

Human bone marrow-derived mesenchymal stem cells (hMSC) were isolated from cancellous bone residues of patients undergoing total hip replacement (written informed consent was given by the patient and as approved by the local ethics committee). Bone debris and bone marrow were mixed thoroughly in

Dulbecco's Modified Eagle's Medium/Ham's F-12 GlutaMAX™-I (DMEM/F12; ThermoFisher, USA) to elute hMSCs. Afterwards, the cell suspension was centrifuged, and the hMSC containing pellet was resuspended in proliferation medium (DMEM/F12, 10% fetal bovine serum (Biochrom, Germany), 1% penicillin–streptomycin (PS; 100 U ml^{-1} penicillin, 0.1 mg ml^{-1} streptomycin; ThermoFisher, USA), 5 ng ml^{-1} basic fibroblast growth factor (bFGF; BioLegend, London, UK)) and seeded into T175 cm^2 flasks (Greiner Bio-One, Frickenhausen, Germany). Non-adherent cells were removed 3–4 d post isolation by carefully washing with PBS, and adherent cells were expanded at 37 °C, 5% CO_2 in proliferation medium, as described above. Finally, hMSCs were detached with 0.05% trypsin-EDTA (ThermoFisher, USA), and seeded at a density of 3–5 × 10^4 cells ml^{-1} into T175 cm^2 flasks.

Cell printing experiments were performed using the alginate-gelatine blend hydrogel formulation, as described above. Alginate and gelatine powders were sterilised by UV irradiation at 254 nm (UVL hand lamp with filter, A. Hartenstein, Würzburg, Germany) with an intensity of 1 mW cm^{-2} for 10 min before dissolving in sterile PBS. hMSC at passage 3 were carefully resuspended at a concentration of 1 × 10^6 cells ml^{-1} in the blend hydrogel with a spatula to avoid the formation of air bubbles. Afterwards, the hydrogel encapsulated cells were either printed using the regulated pressure source from PH1 (CF-300N/H cell-friendly print-head for contact dispensing) and cartridge heater at 30 °C (CF300, RegenHU, Switzerland) through a 100 μm radius needle into cylindrical silicon molds (2 mm deep, 6 mm diameter) using pressures from 1 to 5 bar, or were exposed for 60 s to the same shear rate induced by the rheometer comparable to pressures from 1 to 7 bar and were subsequently crosslinked in a filter-sterilised 2% w/v $CaCl_2$ solution. Cast hydrogels served as a control for cells receiving no shear stress. All constructs were cultured for 24 h at 37 °C, 5% CO_2 in proliferation medium to assess cell viability.

2.6. Cell viability analysis

The viability of hydrogel-encapsulated hMSCs was analysed using calcein acetoxymethyl ester (Calcein-AM; ThermoFisher, USA) to detect viable cells and ethidium homodimer-I (EthD-I; Sigma Aldrich, USA) for detection of dead cells. Cell-laden hydrogels were washed two times with PBS, and were subsequently incubated for 45 min at RT in a staining solution (1 μM EthD-I, 2 μM Calcein-AM) 24 h after cell encapsulation. Following that, constructs were washed with PBS and top view images were taken using an inverted fluorescence microscope (Zeiss AxioObserver.Z1, Carl Zeiss, Germany). Live and dead cells were counted for three samples per condition, at six locations within each sample with Fiji [23]. Finally, the ratio of viable cells in the different constructs was normalised to the viability of cells encapsulated in cast hydrogels, which was set to 100%.

Table 1. Mathematical model parameters. Needle geometry was selected based on the Nordon EFD needles used experimentally. The needle length, L, refers to the true length of the cylindrical metal component of the needle. A full description of the parameter selection process is provided in SI is available online at stacks.iop.org/BF/9/044107/mmedia.

Parameter	Symbol	Selected value/range
Needle length	L	12.22 mm
Needle radius	R	100, 125, 165 μm
Extrusion pressure	Δp	0–5 bar
Average extrusion velocity	$\bar{v}$	1–40 mm s^{-1}

2.7. Mathematical model

The shear thinning behaviour of the sample was characterised by fitting the following Power Law equation to the linear region of the shear rate-viscosity rheology plot for each material (full derivation shown in the SI);

$$\eta = K\dot{\gamma}^{n-1} \tag{1}$$

where η is the viscosity, $\dot{\gamma}$ is the shear rate, and K and n are shear thinning coefficients. The extrusion velocity at a distance, r, across the radius of a needle, R, was calculated using the following equation for a range of materials and printing conditions to examine the theoretical extrusion profile and distribution of shear forces within the needle tip;

$$v = \frac{n}{n+1}\left(\frac{\Delta p}{2LK}\right)^{\frac{1}{n}}\left(R^{\frac{n+1}{n}} - r^{\frac{n+1}{n}}\right). \tag{2}$$

The average extrusion velocity for a range of printing pressures and needle geometries was also calculated;

$$\bar{v} = \left(\frac{-\Delta p}{2LK}\right)\left(\frac{n}{3n+1}\right)R^{\frac{n+1}{n}}. \tag{3}$$

Consistent with the bioprinting set up used experimentally in this investigation, the parameters and limits presented in table 1 were selected.

The Power Law data for 25 wt% poloxamer 407 and printable pre-crosslinked alginate was used along with three hypothetical samples with Newtonian ($n = 1$), weakly shear thinning ($n = 0.6$) and highly shear thinning ($n = 0.2$) properties. To further investigate the forces being experienced on particles, or hypothetical cells within a bioink, the shear rate, $\dot{\gamma}$ (equation (SI2)), shear stress, τ (equation (SI4)) and residence time, t (rearranging equation (2) as $\boldsymbol{v} = \frac{\boldsymbol{L}}{\boldsymbol{t}}$) as a function of needle diameter was also calculated for these materials. It was assumed that each material was extruded using the experimentally derived optimal printing pressure or 2.0 bar for the theoretical fluids, and a 125 μm inner radius needle of length 12.22 mm (this relates to the whole length of the metal tube within the Nordson EFD precision needles; Nordson states these needles to have a length of 0.25' as this is the process relevant length sticking out of the plastic

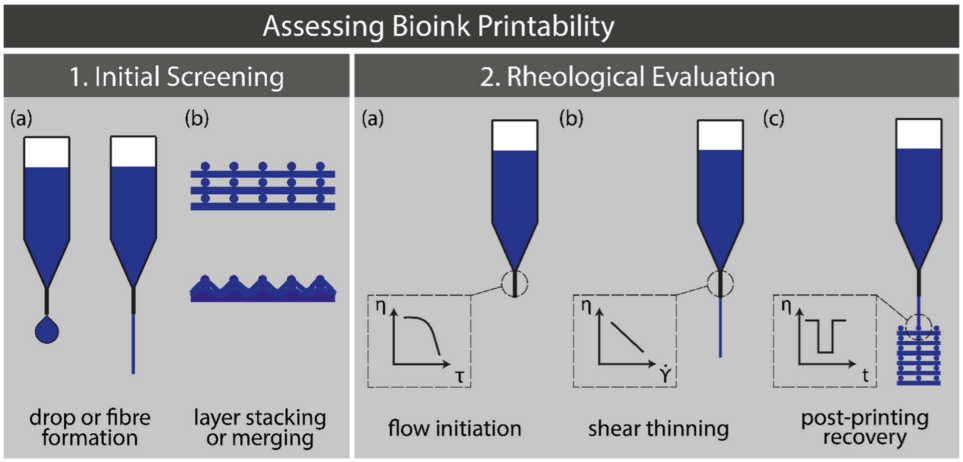

Figure 1. Outline of the proposed research method to assess bioink printability. 1. Initial screening of ink formulations to establish (a) fibre formation as opposed to droplet formation and (b) successful layer stacking without merging between layers. 2. Rheological evaluations are employed to characterise (a) the flow initiation properties and yield stress, (b) degree of shear thinning to predict the extrusion process and cell survival and (c) recovery behaviour of the inks after printing.

Luer-Lock adapter), consistent with those used experimentally.

3. Results and discussion

3.1. Printability assessment and limitations

3.1.1. Outline of characterisation approach and choice of test materials

Inks for bioprinting must fulfil a number of key requirements for processing with a 3D bioprinter [24]. The main challenge is that they need to be printable and meet criteria dictated by their application as products for tissue engineering and regenerative medicine [4]. This work mainly addresses printability issues and we propose a two-step printability assessment (figure 1) to characterise material properties important for printability, and to gain information that helps processing and designing ink materials for biofabrication. The first assessment step, the manual dispensing, is meant to be a simple, reliable initial screening method that focusses on the material´s ability to form fibres, rather than droplets, and the ability for the fibres to stack layer-by-layer to form 3D constructs without merging and does not require a bioprinter or other advanced equipment. The second step requires rheological measurements. Rheology can offer a useful tool to reproducibly gain information about ink properties important for printing if it focuses on the right experiments and if the results are considered holistically. The experiments we chose are meant to describe the inks properties before, during and after being extruded in the printing process. Thus we chose to analyse the material using (a) a shear stress ramp to test if the material exhibits a yield stress, (b) shear viscosity tests to investigate the shear thinning properties of the material and (c) recovery tests applying an alteration of high and low shear rates to the material to see how it recovers after being exposed to high shear rates.

To offer comparability and to validate the hypothesis stated above, the printability assessment was performed on four materials with diverse properties. Accordingly, the materials chosen for this work show different levels of complexity and represent a range of classes of printable materials. One of the best accessible printable materials is Nivea Crème used for body care. It is cheap, has a constant quality and composition, and is an example of a soft colloidal ink. Amongst other products, Nivea Crème, which has been established by bioprinter manufacturing company RegenHU (Switzerland) as demonstration ink, shows very good print fidelity, fulfils the requirements mentioned above and is very well-suited as test ink for 3D bioprinting beginners. Another material displaying successful printing results is poloxamer 407. Its properties highly depend on the concentration in a water-based solution as well as on temperature. Poloxamer 407 is thermoresponsive; while a gel at room temperature, solutions are in a liquid phase below approximately 10 °C and can therefore be used as a sacrificial support network to be washed out and removed from structures easily [25]. Above a critical concentration, this triblock copolymer is highly shear thinning and recovers very quickly after shear stress is removed without the need for external crosslinking. In this work, it was used as test system displaying the importance of concentration on printability. Furthermore, we also consider concentrations that are not printable to show how non-printable materials behave during the screening procedure. A step closer towards inks more appropriate for bioprinting was demonstrated by using alginate solutions. Alginate is one of the most frequently used materials in bioprinting mainly due to its fast, ionic crosslinking via bivalent ions like calcium. Because there are different compositions,

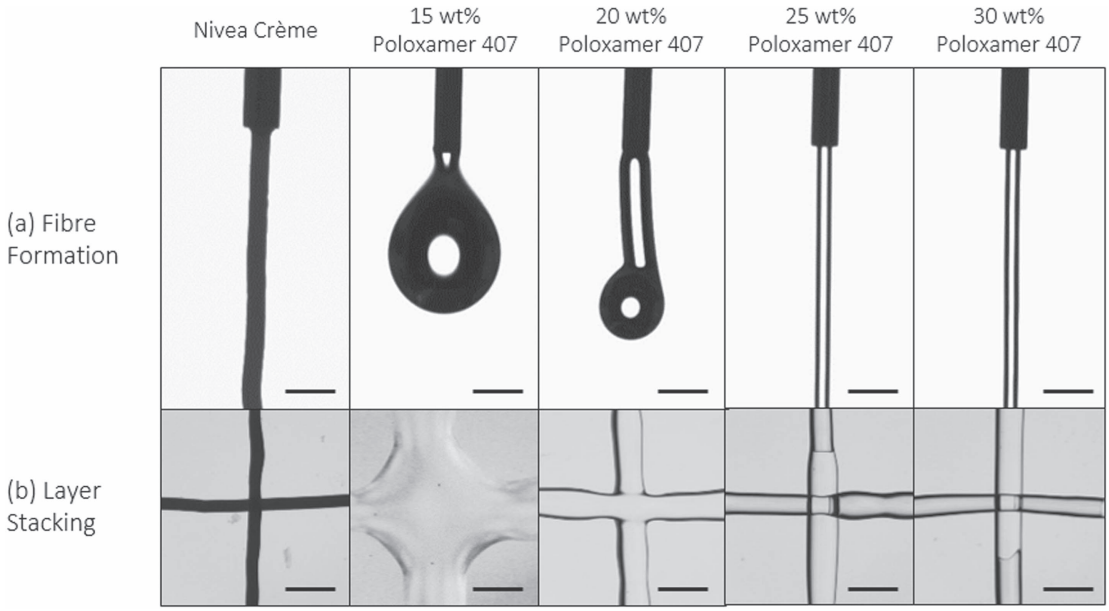

Figure 2. (a) Fibre formation and (b) layer stacking results for Nivea Crème and poloxamer 407 samples, demonstrating that concentrations of poloxamer 407 below 25 wt% are unsuitable for printing due to their inability to form fibres or maintain extruded geometry. Scale bar = 1 mm.

molecular weights and polydispersities available, the rheological behaviour can vary between different sources. For example, surveying a number of alginate-based bioink studies, printable concentrations ranged from 3% to 10% w/v while printing parameters were optimised using pressures between 0.6 and 7.5 bar and 0.21–0.61 mm diameter needles [26–29] with little or no description for the selection procedure. Alginate at higher molecular weights and concentrations is a shear thinning physical gel and it is important to adjust concentrations to achieve printable properties. But as displayed by several reviews [30, 31] there are ways to use various crosslinking strategies (printing into calcium-chloride solutions, spraying a mist of calcium-chloride on the solution exiting the nozzle, pre-crosslinking with calcium-chloride) to process alginate at otherwise unprintable compositions. A recent trend in biofabrication is heading towards multimaterial bioinks [3, 32] because these ink systems can profit from the benefits of different materials. A readily available and well-established composite ink is based on the combination of alginate and gelatine. Alginate allows for fast crosslinking while gelatine makes the material thermoresponsive. In this study, a formulation reported by Wüst *et al* (2015) consisting of a 4% w/v alginate solution mixed in equal parts with a 20% w/v gelatine solution, in a final alginate-gelatine concentration of 2%–10% w/v [22] was used.

3.2. Printability assessment method stage 1: initial screening

3.2.1. Manual dispensing

Preliminary testing can rapidly and effectively demonstrate the ability for a potential ink materials to fulfil two basic requirements for extrusion bioprinting; (a) form consistent, cylindrical fibres and (b) stack layers into coherent structures by examining and comparing the quality of material extruded by hand. Since this process was designed to mimic the bioprinting process, the needle size was selected to match the needle ultimately used during bioprinting. By applying the method to a range of concentrations of poloxamer 407 solution, the difference in fibre forming and stacking behaviour is evident compared to the 'control' Nivea Crème sample (figure 2). Videos demonstrating the difference in fibre formation behaviour are included in the SI.

Nivea Crème exhibited characteristic fibre formation and layer stacking without merging, confirming its reputation as a highly printable sample. The fibres were highly consistent and maintained their shape without breaking or detaching. When overlaid in a cross pattern, the fibres did not merge or blend together nor lose their cylindrical fibre morphology in any way.

The poloxamer 407 samples show a range of unprintable and printable behaviour. The 15 wt% sample displayed droplet formation when extruded by hand and could not form coherent fibres. The 20 wt% solution displayed partial fibre formation, whereby short, inconsistent, droplet-like fibres were observed (see SI for video of extrusion behaviour), however the fibres did not retain their shape when deposited in the cross pattern to maintain a 3D structure. The 25 wt% solution was therefore the lowest concentration to produce coherent fibres and adequately stack layers comparable to the control Nivea Crème material and was therefore selected as the most printable

Table 2. Fibre formation and layer stacking testing for various concentration alginate samples mixed with various concentration $CaCl_2$ samples mixed in 7:3 volume mixing ratio. Shaded cells indicate fibre formation and text indicates for how long the fibres stacked without merging. Unprintable samples are indicated in white (too liquid) or dark grey (too solid).

Alginate concentration (w/v)	$CaCl_2$ concentration (w/v) 0.0%	0.5%	1.0%	1.5%	2.0%
4%			1 s	5 s	
6%		1 s	3 s	5+s	
8%		3 s	5+s		
10%		5 s			

formulation. The higher concentrations performed similarly but required more pressure to extrude the fibres by hand. This is unfavourable compared to lower-pressure extrusion whereby high pressures elicit higher shear stress within the needle tip which may be detrimental to cell survival, as discussed in section 3.3.4.

After a review of recent literature surrounding the bioprinting of alginate-based inks [33–35], a range of alginate solutions between 4% and 10% w/v were screened to optimise for printability. With the addition of a range of concentrations of $CaCl_2$ in a standardised 7:3 volume mixing ratio, partial crosslinking of the alginate solutions was initiated to improve the viscoelastic properties. As such, it was apparent that all the non-crosslinked samples and 4% w/v alginate/0.5% w/v $CaCl_2$ solution sample was unsuitable for printing due to their inability to form cylindrical fibres, and to retain distinct layers when stacked (table 2). Samples of higher viscosity formed fibres and retained their shape before blending with the layer below for varying periods of time, also indicated in the table. For these concentrations, this test allowed the rapid observation of the window in which additional crosslinking methods could be applied to solidify the layers and therefore successfully build 3D constructs. For crosslinking methods which can be rapidly applied, including printing into a mist of crosslinking solution or UV irradiation, the concentrations can be screened for their suitability to retain their morphology for a suitable time period depending on the technical limitations of the method used.

Two samples formed consistent fibres, equivalent to the control Nivea Crème results, and retained their morphology for greater than 5 s. This time was deemed the minimum window required to apply a crosslinking agent and these compositions were therefore deemed 'printable'. Ultimately, at higher concentrations alginate or $CaCl_2$ solution, the samples became too firm to manually extrude through the syringe and these were deemed unprintable. Inhomogeneity of the samples, particularly at higher concentrations of $CaCl_2$, was a limiting factor for processing suitable inks for printing. Where the alginate had not been homogeneously mixed into the $CaCl_2$ solution, firm regions of dense hydrogel interfered with the formation of continuous fibre strands, leading to 'blotchy' fibre deposition.

Between the two 'printable' samples which retained their fibre morphology for longer than 5 s, the 8%/1% (alginate w/v concentration/$CaCl_2$ w/v concentration) sample was observed to have a smoother consistency, due to the reduced $CaCl_2$ concentration and this was therefore the preferred printable sample (hereafter referred to as 8%/1% alginate).

Thermoresponsivity is a property of many inks which can be employed to assist the changes in viscoelastic properties required for successful extrusion and solidification into 3D constructs with high shape fidelity [36]. It is characterised by a change in a material's viscoelastic properties as a result of temperature. For bioprinting, this allows inks to be liquefied for extrusion and then rapidly solidified upon deposition to form stable 3D constructs. A composite ink of alginate and gelatine was selected as a widely used example of a composite, thermoresponsive ink. The thermoresponsivity of gelatine allows for the heated extrusion of a low-viscosity ink onto a cooled plate where it rapidly transitions to a high-viscosity state. The incorporation of alginate also allows for simple crosslinking via the use of $CaCl_2$ solutions. In this study, a formulation reported by Wüst *et al* (2015) was used, which consists of a 4% w/v alginate solution mixed in equal parts with a 20% w/v gelatine solution, in a final alginate-gelatine concentration of 2%–10% w/v [37]. In order to include printability assessment of thermoresponsive systems and, more specifically in our study, to be able to get a feeling for printable compositions of alginate-gelatine, the initial screening approach can be adapted using a cold collector. This modified initial screening method revealed that the alginate-gelatine sample was readily extrudable into fibres and could stack when deposited onto the lid of a petri dish filled with ice, consistent with the widely observed thermoresponsive properties of the gelatine component [38]. Further characterisation of the thermoresponsive

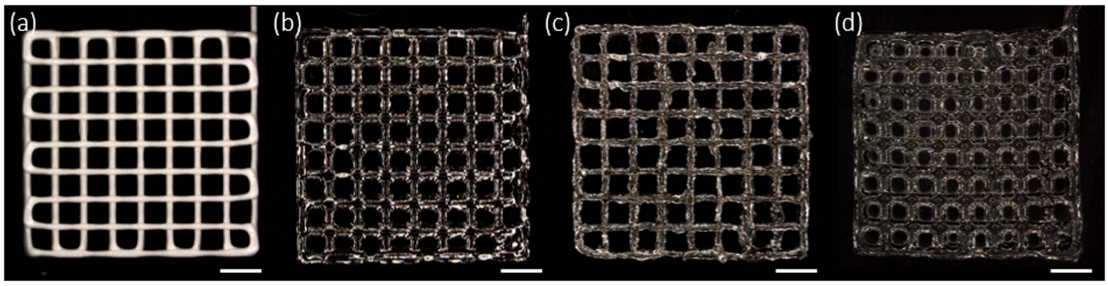

Figure 3. (a) Nivea Crème, (b) 25 wt% poloxamer 407 solution, (c) 8%/1% alginate and (d) 4% w/v alginate-20% w/v gelatine hydrogel scaffolds printed using optimal print conditions selected on the bioprinter. Scaffolds are 12 × 12 mm in dimension with 1.5 mm spacing between fibres and 4 layers high. Scale bar = 2 mm.

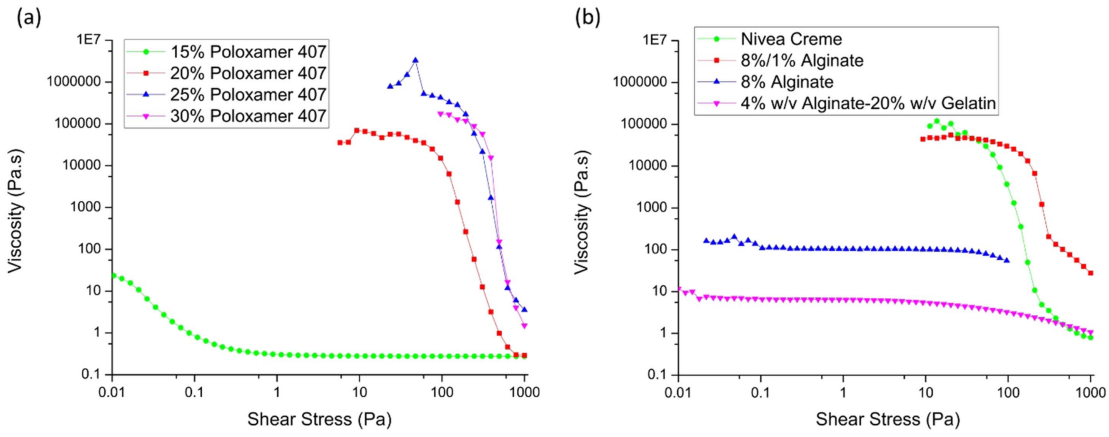

Figure 4. Shear stress ramp data for all experimental samples, performed at 24 °C for all samples except the alginate-gelatine (4% w/v alginate hydrogel, 20% w/v gelatine) which was measured at 37 °C.

properties of the ink to optimise the bioprinting process by choosing the right reservoir and collector temperatures can be performed with a temperature sweep at the rheometer as described in the SI.

3.2.2. Validation of the initial screening process

Currently in literature there is limited reproducibility regarding the selection of bioink formulations, even using the same polymer as discussed in the Introduction. Via the initial screening tests demonstrated above, printable formulations of the different inks were quickly and reproducibly selected based on their ability to form fibres and stable 3D constructs, in some cases with the addition of crosslinking agents. Therefore, this proposed initial screening protocol offers a useful tool to select and compare a range of suitable printable bioink formulations in a reproducible and controlled manner.

To evaluate this screening method, the four printable samples as determined by the initial screening were then successfully bioprinted into 12 × 12 mm crosshatch scaffolds, confirming the efficacy of the initial screening procedure for selecting printable formulations of inks (figure 3).

3.3. Printability assessment method step 2: rheological evaluations

Routine rheology measurements were performed to characterise the yield stress, shear rate-dependent viscosity, and recovery behaviour of the materials. The yield stress can be determined via shear stress ramps. Furthermore, applying the Power Law model to the shear rate-viscosity profiles enabled the estimation of the degree of shear thinning by calculating the parameters n and K for the mathematical model (see SI) and predicting the extrusion behaviour at bioprinting-induced shear rates. Finally, the recovery of the materials after being subjected to shear rates similar to that during bioprinting was evaluated to characterise the window in which crosslinking can be achieved.

3.3.1. Flow initiation analysis: yield stress measurements

To characterise the 'at-rest' viscoelastic behaviour the ink systems tested before, shear stress rheometry was performed. A shear stress ramp offers a useful tool for determining the yield stress of materials. By plotting the viscosity over shear stress, the viscosity at which the material first starts flowing and therefore to approximate its 'at-rest' viscosity could be analysed. The experimental results are shown in figure 4.

Table 3. Results of the pipetting experiment for each of the poloxamer 407 samples and their yield point.

	Yield stress (Pa)
15 wt% poloxamer 407	*
20 wt% poloxamer 407	93.6
25 wt% poloxamer 407	227
30 wt% poloxamer 407	348
Nivea Crème	72.1
8%/1% alginate	166
8% w/v alginate	*
4% w/v alginate-20% w/v gelatine	*

Note. *Material was already flowing at the beginning of the shear stress ramp at 0.01 Pa and therefore the yield point could not be determined.

The yield stress was determined using the intersection point of two tangents, one in the plateau-region of the viscosity where the material is deformed elastically and one in the region where the viscosity drops and the material flows, for the materials that revealed a clear yield stress. The results are summarised in table 3.

The yield stress of each material reveals significant insights into the material printability. Firstly, it allows the characterisation of the yield stress of the material, below which the material behaves like a solid rather than a liquid. A clear distinction between the printable and unprintable materials can be seen in figure 4, whereby the uncrosslinked 8% w/v alginate sample does not exhibit a steep drop in viscosity upon initiation of flow. By comparison, the pre-crosslinked sample has a yield stress over an order of magnitude larger and this indicates the role the pre-crosslinking method plays in improving the rheological properties of ink for printability. Additionally, the printable poloxamer 407 samples also demonstrated significantly higher yield stress points than the unprintable concentrations, and it was also observed that the yield point viscosities for all printable samples are significantly higher than the unprintable samples, above 10 000 Pa s. The shear stress ramp for the alginate-gelatine sample was performed at 37 °C and therefore very low viscosity and yield stress are to be expected compared to the other samples. The printability of alginate-gelatine is strongly dependent on the thermoresponsive increase in viscosity induced by the cooled collector plate. Secondly, these results demonstrate the shear thinning properties of the inks, whereby the viscosity of each material dropped at higher shear conditions. This phenomenon will be characterised further in the following section.

3.3.2. Shear thinning characterisation

The shear viscosity profiles of a range of experimental samples were acquired from the rheology measurements (figure 5). All samples show shear thinning behaviour, characterised by a decrease in viscosity over an increasing shear rate. For many of the samples, the linear trend when plotting the results on double-logarithmic axes can be characterised by applying the Power Law regression (as described in section 2.7) to obtain a quantification of the degree of shear thinning observed. This was later used to predict the behaviour of the materials during dispensing in the bioprinting process.

As shown in figure 5, each material demonstrates shear thinning behaviour, characterised by the decrease in viscosity with increasing shear rate. The 15 wt% poloxamer 407 sample, deemed unprintable in the initial screening, exhibited significantly lower viscosities over the shear rate ramp compared to Nivea Crème as well as the printable concentrations of poloxamer 407, 25 wt% and 30 wt%, which align very closely in shear thinning properties (figure 5(a)).

The shear-viscosity profile for Nivea Crème also demonstrates shear thinning behaviour. However, difficulties in measuring the Nivea Crème sample led to inconsistencies in the shear-viscosity measurements for higher shear rates. Material slipping out between the rheometer plates resulted in an upper measurable limit of 1 s^{-1}. However, consistent shear thinning behaviour following a Power Law trend was observed below approximately 1 s^{-1}.

The effect of the addition of $CaCl_2$ on the 8% alginate solution is evident in the shear-viscosity plot displayed in figure 5(b). The pre-crosslinked sample displayed higher viscosity over the low shear rate range compared to the uncrosslinked sample, which also exhibits a Newtonian plateau below shear rates of approximately 0.3 s^{-1}. Over the full 0.01–2000 s^{-1} shear rate range, the shear thinning behaviour of the pre-crosslinked 8%/1% alginate sample was comparable to that of the 25 wt% and 30 wt% poloxamer 407 samples.

The trend in the shear thinning profiles for the printable samples suggests there may exist a window of required viscosity for the successful extrusion of inks which also satisfy the initial screening conditions. But given that the shear thinning profile for the 20 wt% poloxamer 407 solution compared to the 25 wt% and 30 wt% is similar, one would predict that these materials would have similar printability. However, it was concluded from the initial screening method that the poloxamer 407 material at 20 wt% did not have adequate fibre formation and layer stacking behaviour required for printability. It is therefore important to note that the shear thinning rheology solely measures viscosity under different shear stresses and printability cannot be concluded from these results alone. The rheological explanation for whether a material will form fibres or droplets when extruded through a nozzle is significantly more complex than captured in the shear-viscosity measurements, as this measurement does not fully characterise the effects of other behaviours such as surface tension or dynamic viscoelastic properties.

Nevertheless, the information extracted from the shear-viscosity results can help gaining a better

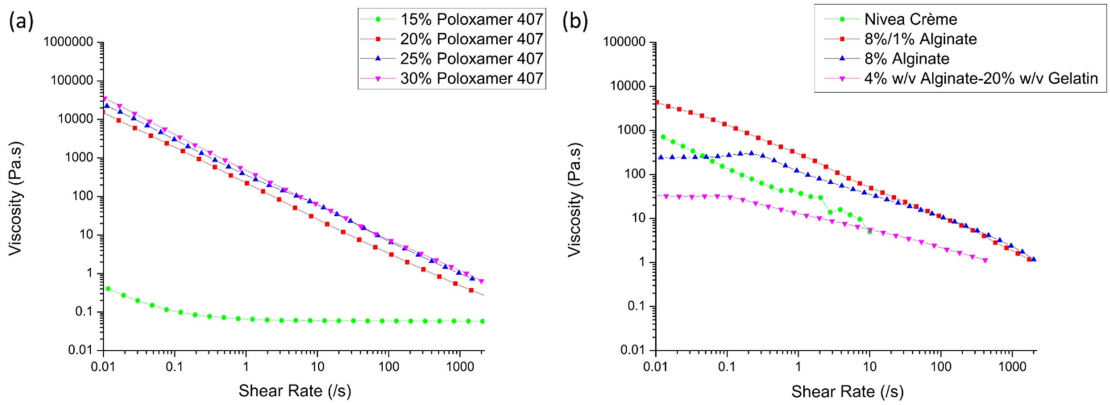

Figure 5. Shear-viscosity results for (a) all poloxamer 407 samples, as well as (b) Nivea Crème, pre-crosslinked 8%/1%, uncrosslinked 8% w/v alginate and the alginate-gelatine sample (4% w/v alginate hydrogel, 20% w/v gelatine).

Table 4. Values of shear thinning coefficients for Nivea Crème, a range of poloxamer 407 samples, 8%/1% pre-crosslinked alginate, uncrosslinked 8% w/v alginate and alginate-gelatine samples, taken from regressions of the linear regions of graphs in figure 5. Inks deemed 'printable' in the initial screening are shown in bold.

Sample	*K*	*n*
Nivea Crème	**26.1**	**0.552**
15 wt% poloxamer 407	0.0622	0.988
20 wt% poloxamer 407	222	0.117
25 wt% Poloxamer 407	**406**	**0.127**
30 wt% poloxamer 407	510	0.102
8%/1% alginate	**254**	**0.307**
8% w/v alginate	130	0.433
Alginate-gelatine	**13.3**	**0.608**

understanding for the material. The main key is to quantify the shear thinning properties of the materials by plotting the viscosity with respect to shear rate on logarithmic axes and applying a Power Law regression in the form of equation (1) to the linear region of the slope. The coefficients, *n* and *K*, were calculated from the regression equations as per table 4. These coefficients can be used to predict possible printing conditions and to analyse the conditions present in the needle during dispensing as will be discussed in the following sections.

3.3.2.1. Window of printability

A common and significantly time-consuming stage in bioink development is the optimisation of ink formulation such that it can be extruded within the operating parameters of a specific bioprinter. Simply put, one must know if a novel hydrogel has the right viscosity such that it can be extruded out of nozzles available to the laboratory and using extrusion pressures achievable by the bioprinter, at a relevant velocity that can be matched to the collector speed. Using a mathematical model, based on shear viscosity measurements, a method to determine an ink's 'window of printability' has been developed and demonstrated for a range of common inks. By modelling the extrusion process, and then limiting the results to within the operating capabilities of the bioprinter used experimentally, the combination of parameters required for successful extrusion, called the 'window' can be calculated.

The theoretical extrusion velocity of a material, described in equation (3), was calculated for a range of needle sizes and printing pressures used experimentally. Equation (3) is based on the Power Law coefficients and needle geometry and applied printing pressure which were chosen to match those achievable using the 3D bioprinter used experimentally. The velocities at each combination of needle radius and printing pressure were calculated in a table (figure 6), demonstrating the theoretical extrusion velocity of the material over the full range of printing conditions. By then selecting values from this table which fall between 1 and 40 mm s^{-1}, velocities equal to the range of collector plate velocities achievable for high shape fidelity printing in feasible printing times (these values are defined based on our experimental expertise and can be adapted based on individual experience), the combinations of printing conditions which will theoretically lead to successful extrusion could be demonstrated. These combinations form the window of printability, displayed in white in figure 6. The regions displayed in red show where the velocity exceeds 40 mm s^{-1}, exceeding the maximum travel speed of the collector used for high shape fidelity prints. The blue sections show where the velocity is lower than 1 mm s^{-1}, which would lead to practically unfeasibly long printing times. A full derivation of equation (3) and selection of the velocity limits in included in the SI. This model, based primarily on the geometry of the needles used experimentally and operating parameters of the printer, can be readily adapted for different materials and printers.

Consistent with its reputation of being a highly printable material, the Nivea Crème window of printability extends well within the range of machine

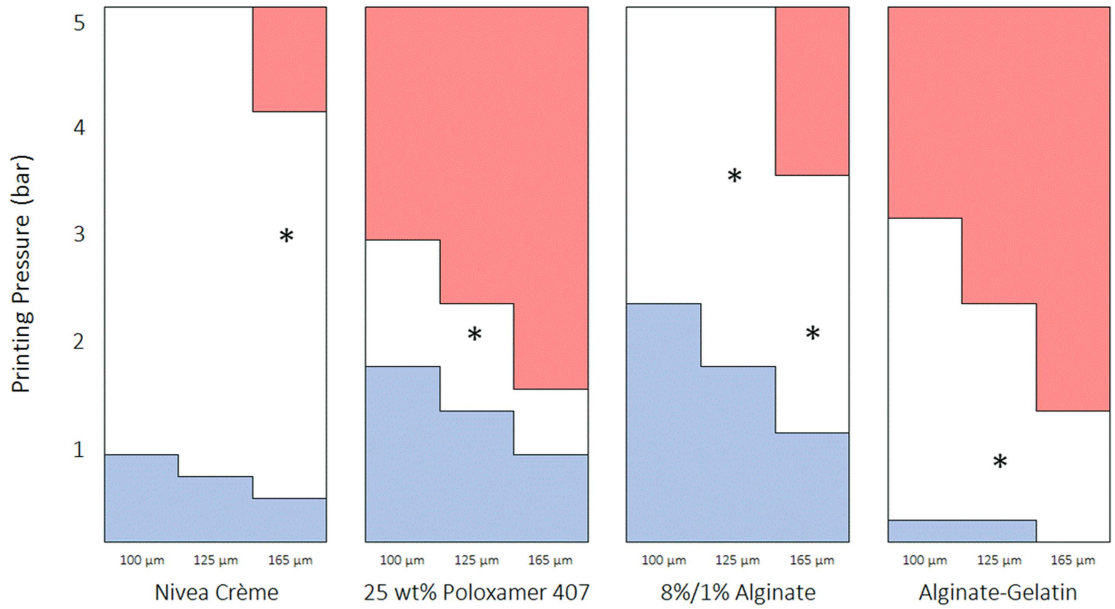

Figure 6. Bioprinting windows calculated for the four printable materials, Nivea Crème, 25 wt% poloxamer 407, 8%/1% alginate and alginate-gelatine inks. The optimal printing parameters (*), found independently, fall within the windows in every case. Red indicates where the extrusion velocity (dependent on the distance from the needle centre and the pressure applied for dispensing) is too high for high shape fidelity printing and blue indicates where the extrusion velocity is too low to achieve a reasonable printing speed.

Table 5. Optimal printing parameters derived experimentally for the four printable samples. The bioprinting shear rates and corresponding viscosities of the materials were also calculated.

Sample	Needle diameter	Printing pressure	Collector velocity	Syringe temp	Collector temp	Bioprinting shear rate, $\dot{\gamma}_b$	Bioprinting viscosity, η_b
Nivea Crème	165 μm	3.0 bar	10 mm s^{-1}	24 °C	24 °C	2652 s^{-1}	0.764 Pa s
25 wt% poloxamer 407	125 μm	2.0 bar	15 mm s^{-1}	24 °C	24 °C	1470 s^{-1}	0.696 Pa s
8%/1% alginate	125 μm	3.5 bar	10 mm s^{-1}	24 °C	24 °C	575 s^{-1}	3.114 Pa s
8%/1% alginate	165 μm	2.0 bar	10 mm s^{-1}	24 °C	24 °C	223 s^{-1}	6.056 Pa s
Alginate-gelatine	125 μm	0.8 bar	10 mm s^{-1}	37 °C	10 °C	279 s^{-1}	1.465 Pa s

operating parameters. Furthermore, the window of printability for 25 wt% poloxamer 407 was calculated, demonstrating a narrow window of printability at pressures between 1.2 and 2.8 bar using different diameter needles. Also, the window of printability for the 8%/1% alginate sample, which was deemed the most successful concentration for printing, demonstrated printability in the initial screening stage. Accordingly, the theoretical model predicts that the sample is printable within a wide range of pressures using any of the needle sizes.

By comparison, the window of printability for unprintable formulations such as the lower concentrations of poloxamer 407 is outside the range of the machine operating parameters. The table is therefore all red, where the white window and blue section would reside at combinations of much narrower needles and lower pressures, and from this alone, it can be predicted that the sample is unprintable. The window of printability therefore offers a rapid guide to the range of parameters in which the material can be successfully extruded.

The size of the window of printability is entirely depending on the shear thinning coefficients, n and K, from the Power Law and vary significantly between materials. From table 4, it is evident that the 25 wt% poloxamer 407 sample has a significantly lower value of n than Nivea Crème and a significantly higher value of K. Combined, this results in a narrower window of printability compared to the other samples which, by comparison, demonstrate acceptable extrusion velocities within the required range over a much larger range of parameters.

To demonstrate the relevance of the theoretical bioprinting window to realistic printing conditions using the printable materials in this study, the parameters selected to successfully print the materials (table 5) were correlated with the bioprinting windows to demonstrate that for every printable material, the optimal parameters fell within the window of printability (figure 6). Additionally, the average bioprinting shear rate, $\dot{\gamma}_b$, was also calculated for each material, by computing the average extrusion velocity, given by equation (3), at the optimal printing conditions, and

substituting this into the non-Newtonian shear rate formula (equation (SI2)) to estimate the shear rate during extrusion. The corresponding viscosity of the material at this shear rate was found by substituting the bioprinting shear rate into the Power Law equation to solve for the bioprinting viscosity, η_b.

In each instance, the experimental bioprinting parameters fall above the centre of the theoretical windows of printability, which correspond to extrusion velocities of approximately 15–20 mm s^{-1}. Since the required collector plate speed for extrusion was lower, this suggests that the model over-estimates the extrusion velocity of the materials but this could also be due to the difficulty in matching between collector speed and extrusion velocity as the bioprinting process can be used to adjust the diameter of the extruded materials strand by changing the printing velocity. The mathematical model was chosen based on a range of assumptions, including friction-free laminar flow and non-slip boundary conditions, both of which would contribute to the over-estimation of extrusion velocity. Therefore, this model acts as a simple, rapid characterisation technique to determine whether a material could be successfully extruded within the operating limits of a bioprinter. Further optimisation of the printing parameters required for ideal construct fabrication is recommended to be carried out on the bioprinter itself.

3.3.2.2. Influence of shear thinning properties on process-relevant conditions within the needle

Using the theoretical extrusion velocity, shear rate, shear stress and residence time equations, a clearer understanding of the theoretical extrusion behaviour of materials inside the needle could be shown. In particular, it allowed us to predict spatial distributions of said parameters inside the needle, for both hypothetical and real bioinks (figure 7). Besides the parameters dictated by the printer setup (needle radius, needle length and pressure applied for dispensing), the profiles shown in figure 7 only depend on the Power Law coefficients n and K gained from the shear viscosity measurements.

These profiles were calculated for three hypothetical samples with Newtonian ($n = 1$), weakly shear thinning ($n = 0.6$) and highly shear thinning ($n = 0.2$) properties (K values calculated using a rearranged form of equation (3) such that average extrusion velocity is equal to 20 mm s^{-1}) at 2 bar printing pressure (figures 7(a), (b)). Similar profiles were calculated for the 25 wt% poloxamer 407 at optimal 2 bar printing pressure (figures 7(c), (d)), and for 8%/1% alginate at optimal 3.5 bar printing pressure (figures 7(e), (f)). These profiles show significant differences in the conditions across the radial axis of 125 μm needles at the respective, representative bioprinting conditions. For all samples, the shear rate increases towards the needle wall. For the poloxamer 407 sample, this effect is concentrated close to the needle wall while for the Newtonian sample, this is a linear relationship. The shear stress, independent of material properties, also increases linearly to a maximum at the needle wall, while the residence time of the material particles demonstrates for how long the material will experience these high shear conditions.

The residence time of theoretical particles evenly distributed within the inks increases exponentially towards the needle wall but varies significantly depending on the material chosen, and therefore on shear thinning behaviour characterised by n and K. To quantify this, the points on the graph correspond to the percentage of theoretical particles, or cells, encapsulated within that radius. From left to right, this corresponds to 0.005%, 10%, 20%, … 80%, 90%, and 95% of cells encapsulated within that radius over the entire length of the needle. For example, for the non-shear thinning Newtonian fluid, the outer 5% of particles at the 95% data point reside at shear stresses of above 0.997 Pa for at least 6.10 s. By comparison, the outer 5% of cells suspended in a highly shear thinning fluid only experience this shear stress for more than only 3.21 s, significantly reducing the application time of harmful shear conditions. For the 25 wt% poloxamer 407 solution, this is just 2.90 s. Considering that all three theoretical materials have the same average extrusion velocity, by reducing the impact of high shear conditions on the cells most at-risk is a significant consideration for the design of shear thinning inks. These results support the findings of other groups, which will be discussed in more detail in the following chapter, by clearly displaying that shear thinning properties of inks protect the cells from high residence times in high shear conditions and thus potentially improve cell survival.

3.3.2.3. Cell printing and viability tests to display the importance of the residence time

The shear forces that emerge within the needle during the printing process have been hypothesised in the literature to have a detrimental effect on cell survival [9, 15]. In response, several key papers have investigated the role of these forces as key to understanding the extrusion processes and potential effects on cell damage [9, 27, 39, 40]. As the profiles in figure 7 demonstrate, not only the shear forces but also the residence time is a crucial factor to be considered during discussions on cell damage by the printing process. Only limited attention was put on this parameter in the data presented to date. Nevertheless, a recent publication by Snyder *et al* (2015) addressed this issue. They used a non-Newtonian extrusion velocity model to calculate the extrusion velocity and residence time of a 2% alginate solution passing through a 150 μm needle for a range of extrusion pressures up to 2.76 bar. These results were then corroborated with experimental trials by printing MSC-laden hydrogels at 1.03 bar and 2.76 bar and comparing the difference in overall viability to an

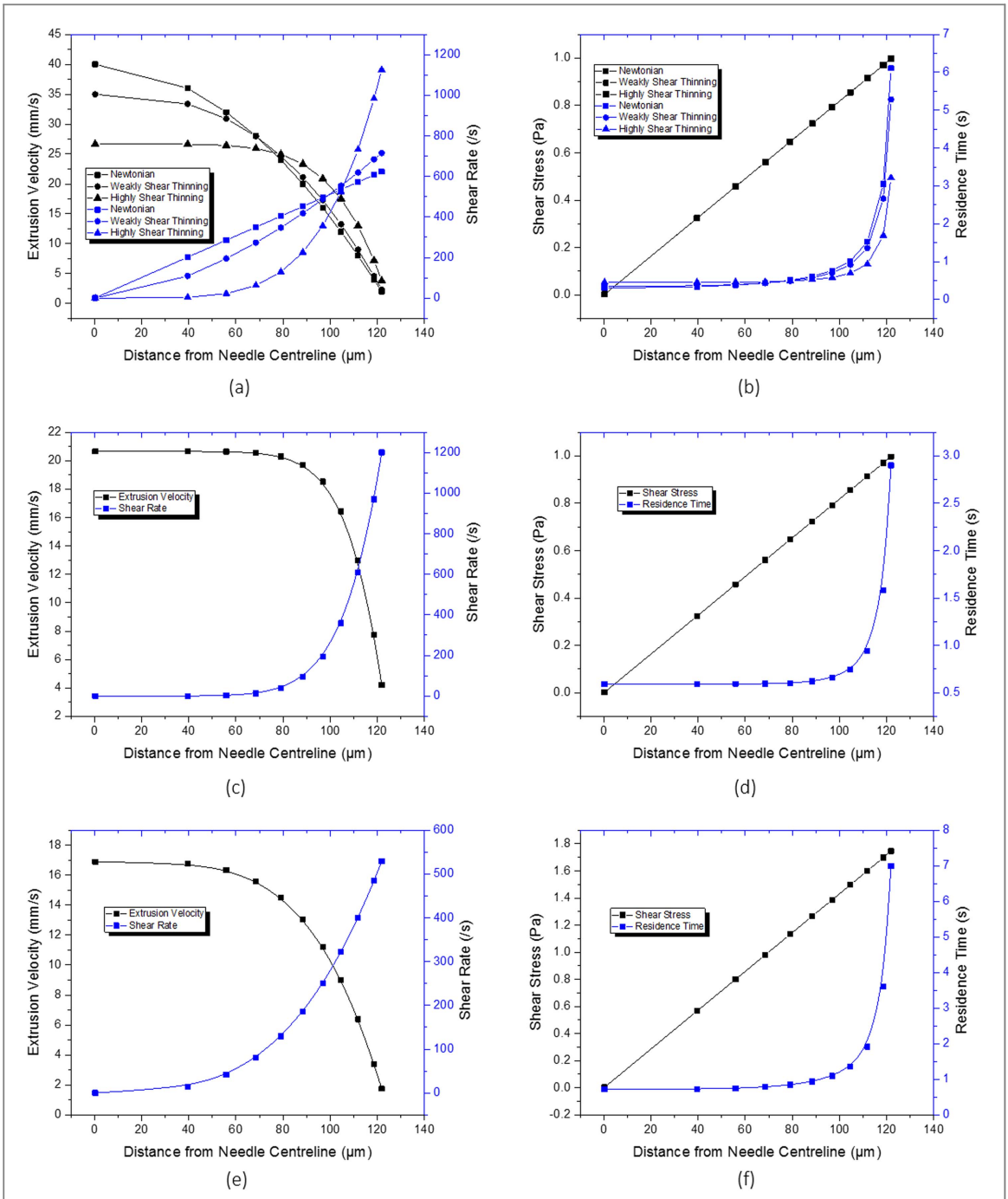

Figure 7. Theoretical extrusion velocity profile across the inner radius of the printing needle for (a) the hypothetical Newtonian, weakly and highly shear thinning fluids, (c) 25 wt% poloxamer 407, and (e) 8%/1% alginate and the shear stress experienced by and residence time of particles within the ink as a function of needle radius for (b) the same hypothetical Newtonian, weakly and highly shear thinning fluids, (d) 25 wt% poloxamer 407, and (f) 8%/1% alginate.

unprinted sample. The study concluded that the increased residence time of the outer-residing cells within the needle tip during printing were adversely affected by the process and this contributed to cell death [16]. To support this hypothesis and highlight the importance of the residence time on cytocompatibility of the printing process, we used the non-Newtonian shear rate and theoretical extrusion velocity model to examine the viability in cell-laden bioinks at shear rates corresponding to extrusion conditions using both the bioprinter and rheometer. Initially, the bioink was extruded using the bioprinter into cylindrical moulds at 1, 3, and 5 bar printing pressure and the viability was determined after 24 h. In parallel, the bioink was loaded in a rheometer and a constant shear rate was applied. To do this, the theoretical average shear rate was calculated for each pressure using a 200 μm diameter needle (table 6). Additionally, the shear rate at 7 bar pressure was also calculated and applied to the ink at the rheometer, although this could not be replicated on the bioprinter. After exposure to this shear rate for 60 s, the samples

Table 6. Printing pressures and the shear rate calculated using the mathematical model (SI) which was applied using a rheometer for 60 s.

Printing pressure	Shear rate
1 bar	22 s^{-1}
3 bar	417 s^{-1}
5 bar	1639 s^{-1}
7 bar*	4035 s^{-1}

Note. *7 bar printing pressure was not possible using the chosen printer setup, however the equivalent shear rate was calculated and trailed using the rheometer.

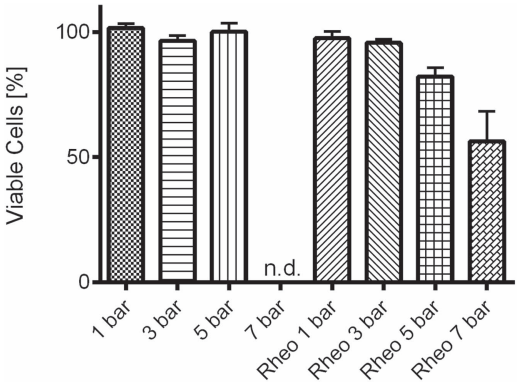

Figure 8. Cell viability data for samples exposed to shear rates induced by increasing bioprinting pressure and constant rotational shear rate rheometry, denoted 'Rheo'. Printing pressure of 7 bar was not achievable with the chosen printer, and therefore no data was available for this condition.

were collected and the viability determined after 24 h to compare to the printed samples.

Interestingly, no considerable reduction in cell viability was observed between the low and high shear samples produced by bioprinting (figure 8) indicating that shear rates up to 1639 s^{-1} did not impact cell viability. Representative live/dead staining images have also been included in the SI. It should be noted that due to the increasing pressure, the flow rate increased significantly between samples and the residence time of the bioink within the needle was very short in the high-pressure regime. In parallel, the viability of samples having experienced the same shear rate induced by the rheometer showed no significant change until shear rates of greater than 5 bar were applied for 60 s. This equates to significantly longer shear application time than that experienced by 99.95% of the sample during extrusion, according to the mathematical model. Therefore, only the outer 0.05% of cells at the needle edge would be susceptible to this level of shear and reduction in cell viability, and would unlikely be apparent in the bioprinting data which displays the average viability of the entire sample.

3.3.3. Recovery behaviour

Recovery testing was undertaken to characterise the behaviour of the materials post-printing. Each of the test materials, including a range of poloxamer 407 concentrations for comparison was initially subjected to a high shear rate of 895 s^{-1} to increase comparability and remove the possibility of material 'memory' of rheological stages. This shear rate was selected as a median value for the theoretical shear rate calculated during extrusion at the optimal print conditions listed in table 5 to assist with comparability between materials. To mimic the shear conditions during printing, the materials were then subjected to a low shear rate of 0.01 s^{-1} to simulate at-rest conditions prior to extrusion, since the rheometer cannot measure viscosity at true zero-shear. Subsequently, a shear rate of 895 s^{-1} was applied to the samples for 100 s to simulate the shear forces in the needle tip during extrusion. And finally, a low shear rate of 0.01 s^{-1} was again applied to measure the recovery of the materials. Consistent with the shear-viscosity measurement, Nivea Crème was unable to be measured due to material slipping out from between the rheometry plates at shear rates above approximately 1 s^{-1}. Also we did not perform these tests on the alginate gelatine samples as these materials requires rapid temperature changes for printability that cannot be mimicked with the rheometer.

Figure 9(a) shows the recovery results for poloxamer 407 concentrations 15–30 wt%. Here, the printable concentration of 25 wt% and also higher-viscosity 30 wt% show rapid recovery after application of the high shear rate. Physically, this allows the material to rapidly increase in viscosity after extrusion and maintain high shape fidelity. By comparison, the unprintable 15 wt% poloxamer 407 sample requires up to 25 s to stabilise in viscosity which would lead to a decrease in retention of cylindrical fibre formation and shape fidelity. However, all poloxamer 407 samples show excellent recovery to their initial viscosity over the 200 s periods, demonstrating no change in polymer structure or properties as a result of exposure to the high bioprinting shear conditions. If other materials do not recover to their original viscosity, permanent material changes may have occurred as a result of the application of a high shear rate. If the high shear rate is chosen to match the approximate shear rate applied during extrusion through a nozzle, these changes could also be evident in the initial screening stages and must be accounted for during material design and selection of crosslinking strategies.

The 8% w/v alginate sample also demonstrates good recovery over the entire 200 s period however a lag in viscosity recovery is observed by the slope in the curve after the drop in shear rate from high to low. In contrast, the pre-crosslinked 8%/1% alginate sample, displays more rapid recovery, reinforcing its suitability as a printable ink over the uncrosslinked sample. Consistent with the shear-viscosity results, the two samples

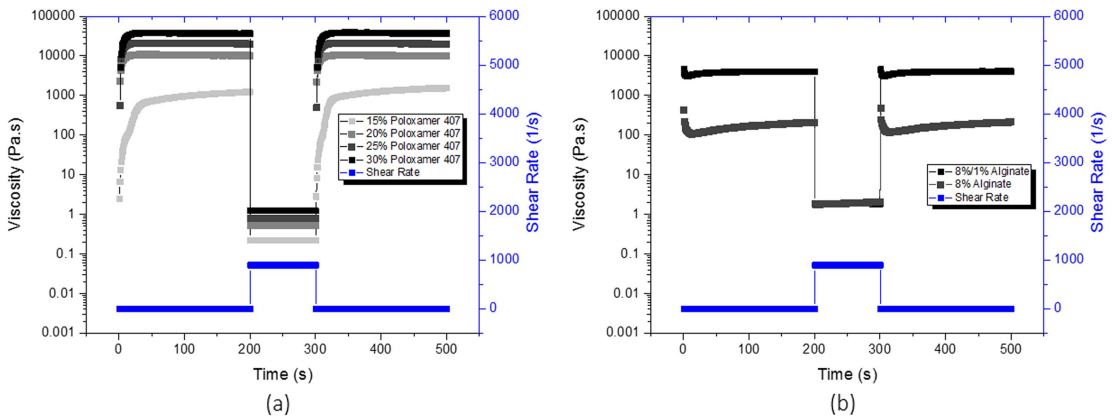

Figure 9. Recovery testing demonstrates the ability for the materials to rapidly recover from the application of a high shear rate (895 s^{-1}) to near-zero shear to simulate the high shear environment experienced by the materials during extrusion printing.

display very similar viscosity at high shear rates (figure 9).

3.3.4. Validation of the rheological evaluations

After presenting the different rheological measurements, clarification surrounding parts of the printability of a range of inks shall be given in a critical evaluation. To do so, the advantages and limitations of each approach will be discussed. The yield stress measurements, demonstrated above, reveal one of the fundamental properties of printable materials as they can show if a material will reduce its viscosity rapidly after a certain shear stress is exceeded. This can be beneficial as it helps to reduce shear rates during printing, above critical shear stress, and at the same time supports shape fidelity at low shear stresses in the elastic region (solid-like behaviour). An additional benefit of the method is that it delivers a clear readout and the yield stress can be determined quantitatively as demonstrated in table 4. However, a disadvantage of this approach is its inability to mimic the printing process as it requires the material to be at rest, ideally be in a steady state. It does not examine the recovery of the material after the internal structure was changed by the extrusion process, which is more interesting for bioprinting. Only if materials exhibiting a yield stress can regain their yield stress quickly after dispensing, printability can be guaranteed. Furthermore, the yield stress should not be too high, as it may impede dispensing as well mixing in of cells [41]. The approach used in this study does not consider dynamics and therefore does not show if a fast shear stress ramp will influence the yield stress.

Shear viscosity measurements performed in the shear rate region as demonstrated in this work (0.01–2000 s^{-1}) can be used to analyse the material properties during extrusion. Their main benefit is that they allow quantification of the dependence of the material viscosity on the shear rate. We could further show that they enable to indicate possible processing parameters such as pressure and needle geometry for a given print speed. In addition, they help to estimate the shear rate that is present in the needle for a given radius and pressure. The recovery measurements shown are also meant to mimic the recovery of the structure of the material after a high shear rate, ideally that predicted by the shear viscosity experiments. It also enables the study of the dynamics of this recovery but as they deliver two values, the time it takes until a certain viscosity is reached and the value of that viscosity, the readout is less clear and at the same time contains one of the main limitations of the approach. The shear rate that mimics at rest conditions is chosen arbitrarily and influences the value of the viscosity at this shear rate which can lead to misinterpretation of the results.

However, the main disadvantage of the complete rheological evaluation is that it did neither enable to define absolute criteria for printability, nor to define quantitative limits for certain measurable parameters. This is mainly due to the nature of rheological evaluations as they display the material parameters at a defined condition and due to the complexity and variety of printable materials as well as possible printing approaches. Nevertheless, we believe that the rheological evaluations demonstrated in this work can contribute to the understanding of what parameters govern printability, and assist in an effective optimisation of materials. In contrast to the initial screening step, rheometry delivers a user-independent assessment. To demonstrate this ability, the results obtained shall be discussed separating them by material rather than evaluation approaches.

Alginate-gelatine was determined to be printable via the initial screening only if printed onto a cooled collector plate. Applicable measurements, yield stress and shear viscosity tests, both support the need for temperature-induced gelation as at 37 °C this material does not display a clear yield stress, and its viscosity was significantly lower than that of the materials deemed printable. In case of pre-cosslinked and non-crosslinked alginate, all steps of the assessment were in

agreement as to the materials' printability. Pre-crosslinked alginate was stated as printable by initial screening and displayed a clear yield stress. Its shear viscosity was in a range comparable with the other printable materials and demonstrated rapid recovery. In contrast, the non-crosslinked alginate sample did not show a clear yield stress and its recovery was slower than that of the pre-crosslinked alginate. At shear rates above 200 s^{-1}, the viscosities of the two alginate inks were similar. As this step only mimics the extrusion process, this is not contradictory to the statement made before. Considering the poloxamer 407 samples at different concentrations, the printability assessment was not altogether conclusive. Although the 15 wt% sample that did not pass the initial screening also showed different rheological properties compared to the printable concentrations (25 and 30 wt%), the 20 wt% sample could also be considered printable if only taking into account the rheological evaluation step. The example of poloxamer 407 reveals two insights. Firstly, the two steps enabled assessment of the printability of the different concentrations and secondly, the rheological behaviour of inks was found to be more complex than can be displayed with the rheological evaluations demonstrated in this work. As we only focus on the viscosity, we do not characterise the elastic behaviour of inks that are known to be viscoelastic materials. We deliberately accepted these limitations as we considering the viscoelastic nature leads to more complicated analysis and we wanted to deliver a clear and simple printability assessment. Nevertheless, we believe that by screening a larger number of potential inks the printability assessment demonstrated in this work can be used to identify criteria for printability.

3.4. Limitations of printability assessment

As the screening process described here is intended to be a simple and easy to reproduce approach, the mathematical model chosen is based on the Power Law model. Although the Power Law is a general and widely accepted model, it has several limitations. Firstly, it is an empirical model for the characterisation of shear thinning materials. This can therefore only be applied to the range of shear rates measured (typically 10^1–10^4 s^{-1}) and cannot be used to describe low and high shear rate behaviour of materials outside of this region [42]. Furthermore, the mathematical model assumes that the fluid flow is steady, linear and that there is no slip between the fluid and the needle wall. It can also only be used for incompressible and time-independent materials. However, the printability assessment process itself is not limited to the use of the Power Law or other assumptions and as such, other models can be implemented. This is important in case the material being developed does not fulfil the requirements mentioned above. For example, Sarker *et al* [10] used the Herschel–Bulkley model that also takes into account low shear rate regions and in addition designed their approach in a way that the model takes into account wall slip and conical needle design. As the Herschel–Bulkley model takes into account the yield stress required to initiate flow, it is particularly useful when applied to flow of deposited material, i.e. retainment of shape fidelity. However, for the exercise of determining appropriate printing parameters above, only higher shear rates are relevant, at which the Herschel–Bulkley model converges to the Power Law. In case of time dependent materials, such as thixotropic materials, the Herschel–Bulkley model can also be adapted for a better fit [43].

There are, of course, a number of other options and experimental techniques to overcome some of the requirements detailed in figure 1. For example, while inks must either shear thin or otherwise decrease in viscosity during printing for successful extrusion, other factors may be implemented to reduce the viscosity of the ink during printing, such as temperature. For example, while alginate-gelatine did not show the required rheological profile at room temperature, by increasing the temperature of the syringe and needle, the required printing viscosity was achieved. Also, if a material does not display the required recovery behaviour, this can be instigated by use of temperature or crosslinking agents to rapidly gel the material to improve the mechanical properties prior to the next layer being printed. The rheological requirements for the use of support structures, *in situ* printing or crosslinking and a variety of other advanced bioprinting methods are not within the scope of this printability assessment method [19, 20]. The rheological requirements of printability, described in figure 1, therefore act as a guide for materials which must be met in combination with many other material and printing factors depending on the type of material and application.

4. Conclusion

In conclusion, the work presented in this paper describes a reproducible method for the assessment of the printability of inks developed for pressure driven, extrusion-based bioprinting. A two-step printability assessment was demonstrated for different materials including non-printable compositions. The first step described an initial screening based on manual material dispensing and focused on the drop or fibre formation properties of the material and on the layer stacking or merging after dispensing. This step already delivered a robust validation of the printability of a material as it addressed the three main properties of a bioink regarding its printability: yield stress, shear thinning and recovery after dispensing. In a second assessment step, these criteria were analysed using rheological evaluations. Yield stress was determined via a stress ramp, the shear thinning properties were

characterised by a shear rate-viscosity plot and fitted using the Power Law model to gain deeper insight into material printability characteristics. Post-printing recovery was analysed via rotational experiments with altered shear rates to simulate the dispensing process. The mathematical model based on rheological data was applied in combination with printer specifications such as pressure, needle properties and print speed, to define a window of printability. This window can help to efficiently develop new ink systems as it displays the parameters the inks can be processed with solely based on the rheological data. Furthermore, the mathematical fit of the shear viscosity data enabled to calculate profiles describing the extrusion velocity, the shear rate, the shear stress and residence time present in the needle during dispensing. These profiles helped to get a clearer understanding of the cell viability rates of printed cell-laden inks compared to those that were stressed at defined conditions using a rheometer. We could show that not only the shear rate but also the residence time of the cells at elevated shear rates need to be considered to improve cell survival. This approach highlighted the need for an integral approach taking into account both the printability and cytocompatibility of the printing process.

Acknowledgments

Naomi Paxton acknowledges the support of the Biofabrication Masters program for providing a mobility stipend, funded by the European Commission and the Australian Governments via the Encounter Program (#2013/3137 001-001 'BIOFAB'). Funding was obtained from the European Union′s Seventh Framework Program (FP7/2007–2013) under grant agreement no. 309962 (Project HydroZONES) as well as the European Research Council under grant agreement 617989 (Design2Heal). We would like to acknowledge Viktor Heinrichs (Anton Paar) for valuable scientific discussion on rheological testing of bioink systems. Furthermore, we would also like to thank Simone Stichler for her assistance in preparing and sterilising bioinks as well as Dr Michael Schmitz for his expertise acquiring images using the contact angle measurement system.

References

[1] Groll J *et al* 2016 Biofabrication : reappraising the definition in an evolving field *Biofabrication* **8** 013001
[2] Rowley J A, Madlambayan G and Mooney D J 1999 Alginate hydrogels as synthetic extracellular matrix materials *Biomaterials* **20** 45–53
[3] Jungst T, Smolan W, Schacht K, Scheibel T and Groll J 2015 Strategies and molecular design criteria for 3D printable hydrogels *Chem. Rev.* **116** 1496–539
[4] Malda J *et al* 2013 25th anniversary article: engineering hydrogels for biofabrication *Adv. Mater.* **25** 5011–28
[5] Murphy S V and Atala A 2014 3D bioprinting of tissues and organs *Nat. Biotechnol.* **32** 773–85
[6] Tian X Y, Li M G, Cao N, Li J W and Chen X B 2009 Characterization of the flow behavior of alginate/hydroxyapatite mixtures for tissue scaffold fabrication *Biofabrication* **1** 45005
[7] Boland T *et al* 2007 Drop-on-demand printing of cells and materials for designer tissue constructs *Mater. Sci. Eng.* C **27** 372–6
[8] Derby B 2010 Inkjet printing of functional and structural materials: fluid property requirements, feature stability, and resolution *Annu. Rev. Mater. Res.* **40** 395–414
[9] Blaeser A, Duarte Campos D F, Puster U, Richtering W, Stevens M M and Fischer H 2016 Controlling shear stress in 3D bioprinting is a key factor to balance printing resolution and stem cell integrity *Adv. Healthc. Mater.* **5** 326–33
[10] Sarker M and Chen X B 2017 Modeling the flow behavior and flow rate of medium viscosity alginate for scaffold fabrication with a 3D bioplotter *J. Manuf. Sci. Eng.* **139** 81002
[11] Kraut G, Yenchesky L, Prieto F, Tovar G E M and Southan A 2017 Influence of shear thinning and material flow on robotic dispensing of poly(ethylene glycol) diacrylate/poloxamer 407 hydrogels *J. Appl. Polym. Sci.* **134** 45083
[12] Rao A 2013 Flow and functional models for rheological properties of fluid foods *Rheology of Fluid, Semisolid, and Solid Foods: Principles and Applications* vol 19 (New York, NY: Springer) pp 27–36
[13] Chen X B and Ke H 2006 Effects of fluid properties on dispensing processes for electronics packaging *IEEE Trans. Electron. Packag. Manuf.* **29** 75–82
[14] Chen X B and Kai J 2004 Modeling of positive-displacement fluid dispensing processes *IEEE Trans. Electron. Packag. Manuf.* **27** 157–63
[15] Chang R, Nam J and Sun W 2008 Effects of dispensing pressure and nozzle diameter on cell survival from solid freeform fabrication–based direct cell writing *Tissue Eng.* A **14** 41–8
[16] Snyder J, Rin Son A, Hamid Q, Wang C, Lui Y and Sun W 2015 Mesenchymal stem cell printing and process regulated cell properties *Biofabrication* **7** 44106
[17] Nair K *et al* 2009 Characterization of cell viability during bioprinting processes *Biotechnol. J.* **4** 1168–77
[18] Li M, Tian X, Kozinski J A, Chen X and Hwang D K 2015 Modeling mechanical cell damage in the bioprinting process employing a conical needle *J. Mech. Med. Biol.* **1515** 1–15
[19] Costantini M *et al* 2017 Engineering muscle networks in 3D GelMA hydrogels: influence of mechanical stiffness and geometrical confinement *Front. Bioeng. Biotechnol.* **5** 22
[20] Ouyang L, Yao R, Zhao Y and Sun W 2016 Effect of bioink properties on printability and cell viability for 3D bioplotting of embryonic stem cells *Biofabrication* **8** 35020
[21] Aguado B A *et al* 2012 Improving viability of stem cells during syringe needle flow through the design of hydrogel cell carriers *Tissue Eng.* A **18** 806–15
[22] Wüst S, Müller R and Hofmann S 2015 3D Bioprinting of complex channels-effects of material, orientation, geometry, and cell embedding *J. Biomed. Mater. Res.* A **103** 2558–70
[23] Schindelin J *et al* 2012 Fiji: an open-source platform for biological-image analysis *Nat. Methods* **9** 676–82
[24] Hölzl K, Lin S, Tytgat L, Van Vlierberghe S, Gu L and Ovsianikov A 2016 Bioink properties before, during and after 3D bioprinting *Biofabrication* **8** 32002
[25] Kang H-W, Lee S J, Ko I K, Kengla C, Yoo J J and Atala A 2016 A 3D bioprinting system to produce human-scale tissue constructs with structural integrity *Nat. Biotechnol.* **34** 312–9
[26] Kang K H, Hockaday L A and Butcher J T 2013 Quantitative optimization of solid freeform deposition of aqueous hydrogels *Biofabrication* **5** 35001
[27] Fedorovich N E *et al* 2012 Biofabrication of osteochondral tissue equivalents by printing topologically defined, cell-laden hydrogel scaffolds *Tissue Eng.* C **18** 33–44
[28] Bakarich S E, Gorkin R, in het Panhuis M and Spinks G M 2014 Three-dimensional printing fiber reinforced hydrogel composites *ACS Appl. Mater. Interfaces* **6** 15998–6006
[29] Detsch R, Sarker B, Zehnder T, Boccaccini A R and Douglas T E L 2014 Additive manufacturing of cell-loaded

alginate enriched with alkaline phosphatase for bone tissue engineering application *BioNanoMaterials* **15** 79–87
[30] Ozbolat I T and Hospodiuk M 2016 Current advances and future perspectives in extrusion-based bioprinting *Biomaterials* **76** 321–43
[31] Dababneh A B and Ozbolat I T 2014 Bioprinting technology: a current state-of-the-art review *J. Manuf. Sci. Eng.* **136** 61016
[32] Chimene D, Lennox K K, Kaunas R R and Gaharwar A K 2016 Advanced bioinks for 3D printing: a materials science perspective *Ann. Biomed. Eng.* **44** 2090–102
[33] Augst A D, Kong H J and Mooney D J 2006 Alginate hydrogels as biomaterials *Macromol. Biosci.* **6** 623–33
[34] Fedorovich N E, De Wijn J R, Verbout A J, Alblas J and Dhert W J A 2008 Three-dimensional fiber deposition of cell-laden, viable, patterned constructs for bone tissue printing *Tissue Eng.* A **14** 127–33
[35] Chung J H Y *et al* 2013 Bio-ink properties and printability for extrusion printing living cells *Biomater. Sci.* **1** 763
[36] Suntornnond R, An J and Chua C K 2017 Bioprinting of thermoresponsive hydrogels for next generation tissue engineering: a review *Macromol. Mater. Eng.* **203** 1600266
[37] Wüst S, Godla M E, Müller R and Hofmann S 2014 Tunable hydrogel composite with two-step processing in combination with innovative hardware upgrade for cell-based three-dimensional bioprinting *Acta Biomater.* **10** 630–40
[38] Schuurman W *et al* 2013 Gelatin-methacrylamide hydrogels as potential biomaterials for fabrication of tissue-engineered cartilage constructs *Macromol. Biosci.* **13** 551–61
[39] Suntornnond R, Tan E, An J and Chua C 2016 A mathematical model on the resolution of extrusion bioprinting for the development of new bioinks *Materials* **9** 756–67
[40] Billiet T, Gevaert E, De Schryver T, Cornelissen M and Dubruel P 2014 The 3D printing of gelatin methacrylamide cell-laden tissue-engineered constructs with high cell viability *Biomaterials* **35** 49–62
[41] Mouser V H M, Melchels F P W, Visser J, Dhert W J A, Gawlitta D and Malda J 2016 Yield stress determines bioprintability of hydrogels based on gelatin-methacryloyl and gellan gum for cartilage bioprinting *Biofabrication* **8** 35003
[42] Rao A 2013 Rheology of fluid, semisolid, and solid foods: principles and applications *Rheology of Fluid, Semisolid, and Solid Foods* vol 19 3rd edn461
[43] De Kee D 1983 Flow properties of time-dependent foodstuffs *J. Rheol.* **27** 581